Axionlike particle search at Higgs factories

Kingman Cheung[1,2,3] and C. J. Ouseph[1,2]

[1]*Department of Physics, National Tsing Hua University, Hsinchu 30013, Taiwan*
[2]*Center for Theory and Computation, National Tsing Hua University, Hsinchu 30013, Taiwan*
[3]*Division of Quantum Phases and Devices, School of Physics, Konkuk University, Seoul 143-701, Republic of Korea*

(Received 30 May 2023; accepted 19 July 2023; published 1 August 2023)

We study the potential of the future Higgs factories, including the ILC, CEPC, and FCC-ee with $\sqrt{s} = 240$–250 GeV on discovering axionlike particles (ALPs) through various production channels in the leptonic final states, $e^+e^- \to f\bar{f}a$, where $f = e, \mu, \nu$. We show that the $e^+e^- \to e^+e^-a$ with $a \to \gamma\gamma$ provides the best bounds for the $g_{a\gamma\gamma}$ and g_{aZZ} couplings, while $e^+e^- \to \nu\bar{\nu}a$, with $a \to \gamma\gamma$ offers the best bounds for the g_{aZZ} and $g_{aZ\gamma}$ couplings. The $e^+e^- \to \mu^+\mu^-a$ with $a \to \gamma\gamma$ provides intermediate sensitivity to the g_{aZZ} coupling. Our estimates of the bounds for the $g_{a\gamma\gamma}$, $g_{aZ\gamma}$, and g_{aZZ} couplings as a function of ALP mass (M_a) ranging from 0.1 to 100 GeV provide valuable insights for future experiments aiming to detect ALPs. We find that $g_{a\gamma\gamma}$ around 1.5×10^{-4} GeV^{-1} for $M_a = 0.1$–6 GeV is currently not ruled out by any other experiments.

DOI: 10.1103/PhysRevD.108.035003

I. INTRODUCTION

The strong *CP* problem in the standard model (SM) is a long-standing problem [1]. The best solution comes by introducing a global $U(1)_{PQ}$ symmetry, which was spontaneously broken down by a dynamical axion field. The resulting pseudo-Nambu-Goldstone boson is known as the QCD axion [1–3]. It can also serve as a dark matter candidate [4–6].

Nonobservation of the neutron electric dipole moment demands the breaking scale of the Peccei-Quinn (PQ) symmetry to be very high with $f_a > 10^9$ GeV, implying a tiny mass to the axion and very small couplings to the SM particles. If we do not require the pseudo-Nambu-Goldstone boson to be the solution of the strong *CP* problem, the mass of the axion is not restricted by the breaking scale f_a. Such a hypothetical particle, coined as an axionlike particle (ALP), is also a pseudoscalar boson.

However, the ALP remains one of the possible dark matter candidates. The ALP as a dark matter candidate is not the motivation of this work, unless the couplings of the ALP are extremely small such that the lifetime is longer than the age of the Universe. On the other hand, the ALP as a low-scale inflaton is a possibility that the ALP can decay [7].

The axion mass and couplings to SM particles can extend over many orders of magnitude, which are only constrained by astrophysical and cosmological observations, as well as collider experiments. In this work, we consider the potential sensitivities on the parameter space of the ALP model by searching for such ALPs in the proposed Higgs factories, including the International Linear Collider (ILC) [8], CEPC [9], and FCC-ee [10] with $\sqrt{s} = 240$–250 GeV. We consider the following leptonic production channels $e^+e^- \to f\bar{f}a$ with $f = e, \mu, \nu$. Given the center-of-mass energy is only 250 GeV, we consider the ALP mass in the range of 0.1–100 GeV. Typical Feynman diagrams for production can be found in Fig. 1.

We focus on the diphoton decay mode of the ALP, which is shown to be dominant. Thus, we have rather clean final states $f\bar{f}(\gamma\gamma)$ with $f = e, \mu, \nu$. The SM background is calculated and found to be small. Finally, we show the sensitive regions of the couplings. A similar study was carried out in [11] at CLIC and FCC, exploring higher center-of-mass energies ($\sqrt{s} = 380, 1500, 3000$ GeV). The focus of their study was on the production of ALP through $e^+e^- > \gamma a, Za$, and $(a \to \gamma\gamma, a \to l^+l^-)$, and specifically on the ALP leptonic, ALP-$\gamma\gamma$, ALP-Zh, and ALP-ah couplings. In our study, we focused on the production of ALP through $e^+e^- \to f\bar{f}a, (a \to \gamma\gamma)$, where $f = e, \mu, \nu$, and also considered the production through the vector boson fusion channels (Fig. 1) and others. Additionally, we

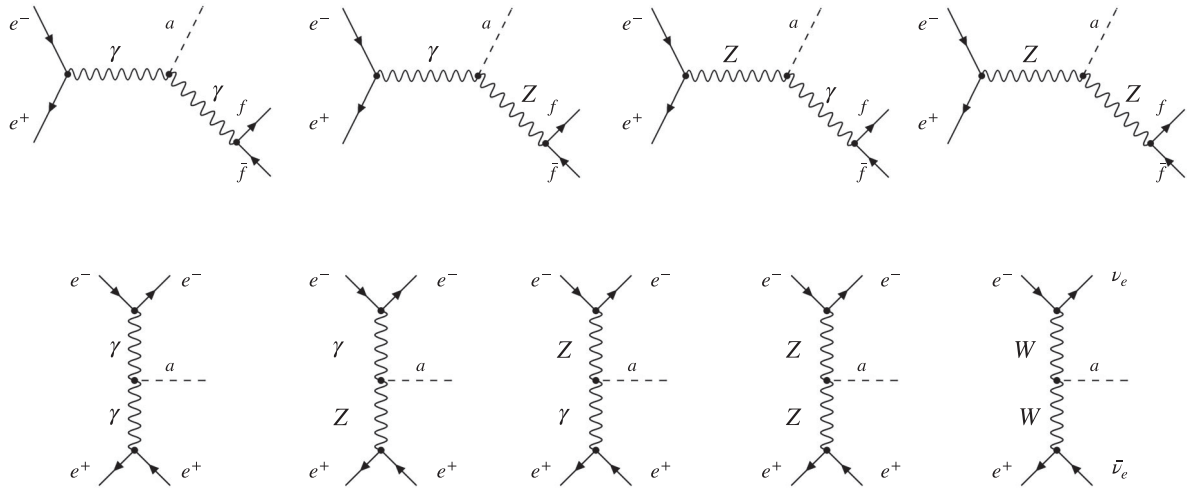

FIG. 1. Typical Feynman diagrams for production of axionlike particles a via the process $e^+e^- \to f\bar{f}a$ at e^+e^- collisions, where $f = e, \mu, \nu$.

extended our investigation to identify the impact of the $g_{aWW}, g_{aZ\gamma}$, and g_{aZZ} couplings. Our specific focus was on the center-of-mass energy of $\sqrt{s} = 250$ GeV.

The organization of this work is as follows. In the next section, we describe the model and existing constraints. In Sec. III, we show the signal-background analysis. We calculate the sensitivities of the ALP couplings in Sec. IV. We summarize in Sec. V.

II. THEORETICAL SETUP

A. Model

The axion, as a pseudo-Goldstone boson, has derivative couplings to fermions, as well as CP-odd couplings to the gauge field strengths. Before rotating the B and W^i fields to the physical $\gamma, Z, W^\pm$, the interactions of the axion are given by [12–14]

$$\mathcal{L} = \mathcal{L}_f + \mathcal{L}_g + \mathcal{L}_{BB} + \mathcal{L}_{WW}, \tag{1}$$

where

$$\mathcal{L}_f = -\frac{ia}{f_a}\sum_f g_{af} m_f^{\rm diag} \bar{f}\gamma_5 f,$$
$$\mathcal{L}_g = -C_g \frac{a}{f_a} G^A_{\mu\nu}\tilde{G}^{\mu\nu,A},$$
$$\mathcal{L}_{BB} = -C_{BB}\frac{a}{f_a} B_{\mu\nu}\tilde{B}^{\mu\nu},$$
$$\mathcal{L}_{WW} = -C_{WW}\frac{a}{f_a} W^i_{\mu\nu}\tilde{W}^{\mu\nu,i},$$

where a represents the ALP field, f_a is the ALP decay constant, $A = 1, \ldots 8$ is the $SU(3)$ color index and $i = 1, 2, 3$ is the $SU(2)$ index. The B, W^3 fields rotated into γ, Z by

$$\begin{pmatrix} W^3_\mu \\ B_\mu \end{pmatrix} = \begin{pmatrix} c_w & s_w \\ -s_w & c_w \end{pmatrix}\begin{pmatrix} Z_\mu \\ A_\mu \end{pmatrix}, \tag{2}$$

where c_w, s_w are cosine and sine of the Weinberg angle. The axion interactions with the fermion and the physical gauge bosons are given by

$$\begin{aligned}\mathcal{L} = &-\frac{ia}{f_a}\sum_f g_{af} m_f^{\rm diag}\bar{f}\gamma_5 f - C_g\frac{a}{f_a}G^A_{\mu\nu}\tilde{G}^{\mu\nu A} \\ &-\frac{a}{f_a}[(C_{BB}c_w^2 + C_{WW}s_w^2)F_{\mu\nu}\tilde{F}_{\mu\nu} \\ &+(C_{BB}s_w^2 + C_{WW}c_w^2)Z_{\mu\nu}\tilde{Z}_{\mu\nu} \\ &+2(C_{WW} - C_{BB})c_w s_w F_{\mu\nu}\tilde{Z}_{\mu\nu} + C_{WW}W^+_{\mu\nu}\tilde{W}^{-\mu\nu}].\end{aligned} \tag{3}$$

The dimensionful couplings associated with ALP interactions from (3) is given by

$$g_{a\gamma\gamma} = \frac{4}{f_a}(C_{BB}c_w^2 + C_{WW}s_w^2), \tag{4}$$

$$g_{aWW} = \frac{4}{f_a}C_{WW}, \tag{5}$$

$$g_{aZZ} = \frac{4}{f_a}(C_{BB}s_w^2 + C_{WW}c_w^2), \tag{6}$$

$$g_{aZ\gamma} = \frac{8}{f_a}s_w c_w (C_{WW} - C_{BB}). \tag{7}$$

B. Existing constraints on ALPs

The experimental bounds on the couplings of ALP to gluons, photons, weak gauge bosons, and fermions have been thoroughly investigated in numerous sources [15–28],

including their effects at colliders when f_a is approximately at the TeV scale [21,29]. Moreover, more recent works had constrained the coupling of ALPs to the $W\pm$ gauge boson can be found in Refs. [30,31].

(1) The LEP and the current LHC experiments can probe a significant region of parameter space for ALPs with mass $M_a \geq 5$ GeV. The LEP utilized the $e^+e^- \to \gamma a, (a \to \gamma\gamma)$ and $Z \to a\gamma$ processes [29] to search for ALPs, while ATLAS and CMS employed the process $\gamma\gamma \to a \to \gamma\gamma$ in PbPb collisions at the LHC [32]. In addition, the rare decay of the Higgs boson $h \to Za, (a \to \gamma\gamma)$ and $h \to aa \to (\gamma\gamma)(\gamma\gamma)$ at the LHC [33] had been utilized to explore the ALP-photon coupling $g_{a\gamma\gamma}$ in relation to the ALP mass M_a.

(2) The ALPs with masses below the MeV scale has been extensively studied in cosmological and astrophysical observations, which have resulted in numerous constraints on ALP couplings, including big bang nucleosynthesis, cosmic microwave background, and supernova 1987A [17,34]. Furthermore, light ALPs can potentially become the cold dark matter [4–6], which could lead to their detection through various astrophysical and terrestrial anomalies [35], such as the unexpected x-ray emission line at around 3.5 keV [36]. These results demonstrated the importance of further exploration and investigation into the properties and behavior of ALPs.[1]

(3) In the mass range of MeV to GeV, ALPs can significantly impact low-energy observables in particle physics. Recent studies in the intensity frontier [31,40–42] have explored numerous potential search avenues. Examples include lepton-flavor-violating decays [43], rare meson decays [31,40,44,45], and ALP production in beam dump experiments [46]. Furthermore, this range of ALPs has been proposed as a possible explanation for the muon anomalous magnetic moment [41,47] and may also provide a feasible solution to the Koto anomaly [48]. These findings highlight the importance of continued research into ALPs and their potential implications in particle physics.

(4) The search for the process $e^+e^- \to \gamma a$ with $a \to \gamma\gamma$ has recently been conducted by Belle II [49] for the ALP mass ranging between 0.1 and 10 GeV. The data utilized in this search corresponded to an integrated luminosity of $(445 \pm 3)pb^{-1}$, and the mass range explored was 0.2 GeV $< M_a <$ 9.7 GeV.

[1]In 2020, an excess in electronic recoil events in XENON1T [37] was reported by the XENON Collaboration. The ALP was a plausible explanation for the excess [38]. However, the same collaboration reported the update with XENONnT [39] that, with an exposure of 1.16 ton-years, no excess above background was observed and thus ruled out the previous excess in XENON1T.

TABLE I. A few proposals of e^+e^- colliders running as a Higgs factory, at which the center-of-mass energy and integrated luminosity are shown.

e^+e^- collider	$\sqrt{s}$ (GeV)	Integrated luminosity (fb^{-1})
ILC	250	2000
CEPC	240	5600
FCC-ee	250	5000

(5) The process $e^+e^- \to e^+e^-a$ with $a \to \gamma\gamma$ at ILC has recently been studied in Refs. [50–52]. Reference [51] showed that the ILC running at $\sqrt{s} =$ 250 or $\sqrt{s} = 500$ GeV can discover ALPs in this range of masses with significantly smaller couplings to the SM than previous experiments, down to $g_{aBB} = 10^{-3}$ TeV^{-1}. Reference [50] showed that with more than 10^9 Z bosons produced in the Giga-Z mode of the future ILC experiment equipped with the high granular nature of the detector, one can discover of the ALPs coupled to hypercharge with couplings down to nearly 10^{-5} GeV^{-1} over the mass range from 0.4 to 50 GeV.

A few proposals of Higgs factories are put forward, including the ILC [8], CEPC [9], and FCC-ee [10], running at center-of-mass energies at $\sqrt{s} = 240$–250 GeV with the nominal luminosities shown in Table I. One of the main goals is to carry out the precision study of the Higgs boson couplings. We investigate the potential search for ALPs e^+e^- collisions at the Higgs factories. Without loss of generality, we choose $\sqrt{s} = 250$ GeV and a conservative integrated luminosity of 2 ab^{-1}.

At the Higgs factories, the leptonic processes that we consider are $e^+e^- \to f\bar{f}a$ where $f = e, \mu$, or ν, followed by $a \to \gamma\gamma$. This study explores the effects of the coupling $g_{a\gamma\gamma}, g_{a\gamma Z}, g_{aZZ}, g_{aWW}$ on the production rates of the ALP. Typical contributing Feynman diagrams are shown in Fig. 1. Among the diagrams, there are s- and t-channel diagrams with the ALP bremsstrahlung off an internal γ, Z, or W propagator.

III. SIGNAL VERSUS BACKGROUND

We use MadGraph5aMC@NLO [53,54] to generate events for the production of ALPs at e^+e^- collisions. We consider the following channels for detecting the ALP signal:

(1) $e^+e^- \to e^+e^-a$ with $a \to \gamma\gamma$

To obtain the production cross sections of the ALP with mass from $M_a = 0.1$ to 100 GeV, we apply the following initial cuts on the transverse momentum p_T^e and rapidity $|\eta^e|$ of the electrons in the final state, as well as the transverse momentum p_T^γ and rapidity $|\eta^\gamma|$ of the photons in final state:

TABLE II. The ALP coupling strengths $g_{a\gamma\gamma}$, $g_{aZ\gamma}$, g_{aZZ}, and g_{aWW} with $C_{WW} = 2$, $C_{BB} = 1$, $f_a = 10^3$ GeV using Eqs. (4)–(7).

ALP couplings	Numerical value (GeV^{-1})
$g_{a\gamma\gamma}$	4.88×10^{-3}
$g_{aZ\gamma}$	1.38×10^{-3}
g_{aZZ}	7.11×10^{-3}
g_{aWW}	8×10^{-3}

(i) $p^e_{T\,\text{min}} = 10$ GeV
(ii) $|\eta^e_{\text{max}}| = 1.83$ ($|\cos\theta_e| < 0.95$)
(iii) $p^\gamma_{T\,\text{min}} = 10$ GeV
(iv) $|\eta^\gamma_{\text{max}}| = 2.5$

(2) $e^+e^- \to \mu^+\mu^- a$ with $a \to \gamma\gamma$
The final state consisting of muons ($\mu\pm$) and a pair of photons from the ALP decay are selected using the same cuts as the electron case:
(i) $p^\mu_{T\,\text{min}} = 10$ GeV
(ii) $|\eta^\mu_{\text{max}}| = 1.83$ ($|\cos\theta_\mu| < 0.95$)
(iii) $p^\gamma_{T\,\text{min}} = 10$ GeV
(iv) $|\eta^\gamma_{\text{max}}| = 2.5$

(3) $e + e^- \to \nu\bar{\nu}a$ with $a \to \gamma\gamma$
Here the ALP is produced along with neutrinos in the final states are selected using the following cuts on the rapidity and transverse momentum of the photon and missing transverse energy of E_T:
(i) $\not{E}^{\text{min}}_T = 20$ GeV
(ii) $p^\gamma_{T\,\text{min}} = 10$ GeV
(iii) $|\eta^\gamma_{\text{max}}| = 2.5$

The corresponding irreducible background is also subject to the same cuts as discussed above. We use $C_{WW} = 2$, $C_{BB} = 1$, and $f_a = 1$ TeV in calculating the ALP cross sections, so the corresponding coupling strengths $g_{a\gamma\gamma}$, $g_{aZ\gamma}$, g_{aZZ}, and g_{aWW} are obtained using Eqs. (4)–(7) and listed in Table II. Note that we have chosen different values for C_{WW} and C_{BB}, otherwise $g_{aZ\gamma}$ would vanish.

We generated 10^5 events using MadGraph5aMC@NLO. The scattering cross section associated with the process $e^+e^- \to f\bar{f}a$ is presented in Fig. 2, where $f = e, \mu, \nu$. We have computed the cross sections using the coupling strengths listed in Table II. Among the three signal processes, $e^+e^- \to \nu\bar{\nu}a$ has the largest cross sections, as it consists of three flavors of neutrinos. On the other hand, $e^+e^- \to \mu^+\mu^- a$ gives the smallest cross sections. For M_a ranging from 0.1 to 10 GeV, the cross section curves remain flat. As M_a increases from 10 GeV, the cross sections gradually decrease, because the final state phase space becomes limited with increasing ALP mass. This pattern is consistent across all three channels.

To suppress the irreducible background, we apply a cut on the transverse momentum of the photon pair. In Fig. 3, we compare the transverse momentum of the photon pair for $M_a = 0.1$–100 GeV with the corresponding

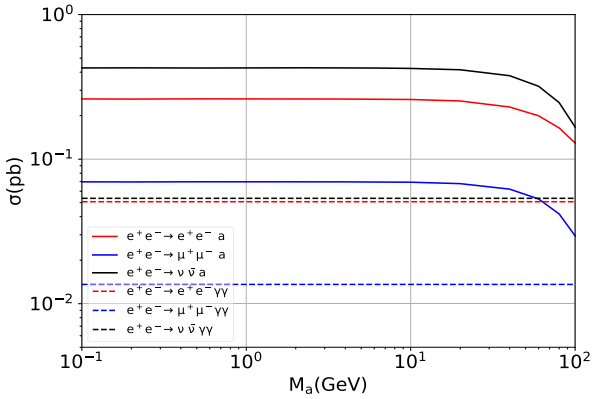

FIG. 2. The ALP signal and SM cross sections at the Higgs factory with $\sqrt{s} = 250$ GeV. Signal cross sections are calculated with the coupling strengths listed in Table II: $g_{a\gamma\gamma} = 4.88 \times 10^{-3}$ GeV^{-1}, $g_{aZ\gamma} = 1.38 \times 10^{-3}$ GeV^{-1}, $g_{aZZ} = 7.11 \times 10^{-3}$ GeV^{-1}, and $g_{aWW} = 8 \times 10^{-3}$ GeV^{-1}.

background. A selection cut of $p_{T_{\gamma\gamma}} > 50$ GeV can suppress the SM background. Total signal and background (BG) event count before and after $PT_{\gamma\gamma} > 50$ GeV is shown in Tables III–VI.

IV. SENSITIVITY ON THE ALP MODEL

The number of signal events N_T at e^+e^- colliders with $\sqrt{s} = 250$ GeV is estimated as

$$N_T = \sigma(e^+e^- \to f\bar{f}a) \times B(a \to \gamma\gamma) \times \frac{N(p_{T_{\gamma\gamma}} > 50\ \text{GeV})}{N_{\text{sim}}} \times \mathcal{L}, \tag{8}$$

where $\sigma(e^+e^- \to f\bar{f}a)$ is the ALP production cross section, $B(a \to \gamma\gamma)$ is the branching ratio of the ALP to a pair of photons (see the Appendices), $N(p_{T_{\gamma\gamma}} > 50\ \text{GeV})$ is the number of events surviving the $p_{T_{\gamma\gamma}} > 50$ GeV cut, and N_{sim} is the total number of events simulated. In this study, we generated $N_{\text{sim}} = 10^5$ events using MadGraph5 aMC@NLO and $\mathcal{L}$ is the integrated luminosity, which we conservatively choose $\mathcal{L} = 2$ ab^{-1}. Similarly, the number of background events N^{SM}_T is estimated as

$$N^{\text{SM}}_T = \sigma(e^+e^- \to f\bar{f}\gamma\gamma) \times \frac{N(p_{T_{\gamma\gamma}} > 50\ \text{GeV})}{N_{\text{sim}}} \times \mathcal{L}. \tag{9}$$

The number of signal events N_T is proportional to the square of the ALP coupling strength g. In this study, we consider all possible ALP interactions encoded in Eq. (3), from all possible channels of ALP production listed in Fig. 1. The bound on the ALP coupling as a function of ALP mass can be obtained by requiring the significance $Z > 2$. The significance Z is defined as [55] (a derivation of the formula is put in Appendix B):

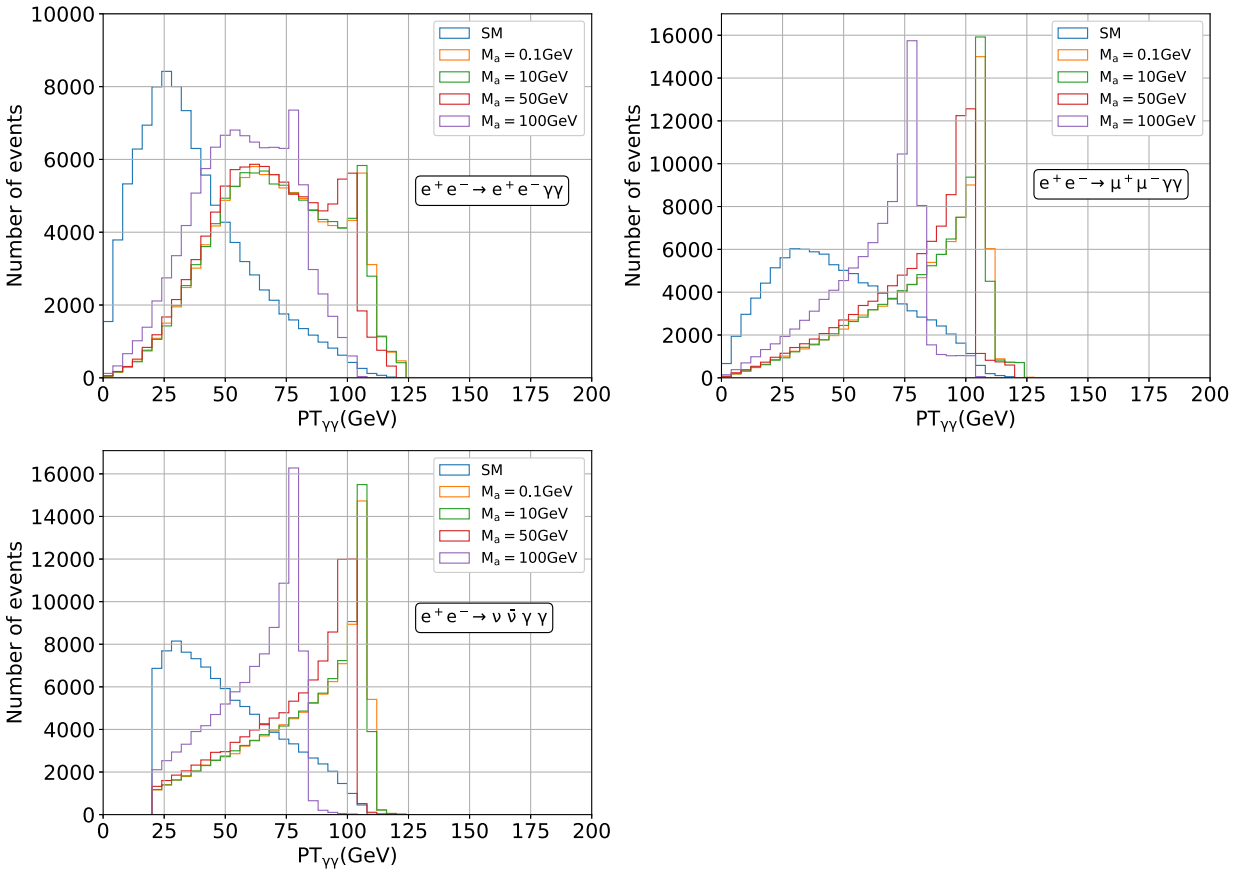

FIG. 3. Transverse momentum $p_{T_{\gamma\gamma}}$ distributions of the photon pair for the signal processes with $M_a = 0.1$–100 GeV and the corresponding SM background at e^+e^- colliders with $\sqrt{s}= 250$ GeV.

TABLE III. Exploring ALP-ZZ vertex: Total signal and BG event count before and after $PT_{\gamma\gamma} > 50$ GeV with $g_{aZZ} = 7.11 \times 10^{-3}$.

	$e^+e^- \to e^+e^-\gamma\gamma$		$e^+e^- \to \mu^+\mu^-\gamma\gamma$		$e^+e^- \to \nu\bar{\nu}\gamma\gamma$	
	Before cut	After cut	Before cut	After cut	Before cut	After cut
BG	101540	26225	27200	12269	107200	49727
$M_a = 0.1$ GeV	112632	88472	111035	97038	731052	631833
$M_a = 1$ GeV	111292	88318	109871	96172	725013	625940
$M_a = 10$ GeV	102134	80226	100580	87976	660434	570575
$M_a = 100$ GeV	46895	29852	45951	34925	288335	214152

TABLE IV. Exploring ALP-$Z\gamma$ vertex: Total signal and BG event count before and after $PT_{\gamma\gamma} > 50$ GeV with $g_{aZ\gamma} = 1.38 \times 10^{-3}$.

	$e^+e^- \to e^+e^-\gamma\gamma$		$e^+e^- \to \mu^+\mu^-\gamma\gamma$		$e^+e^- \to \nu\bar{\nu}\gamma\gamma$	
	Before cut	After cut	Before cut	After cut	Before cut	After cut
BG	101540	26225	27200	12269	107200	49727
$M_a = 0.1$ GeV	17143	13465	14424	12606	89868	77671
$M_a = 1$ GeV	16972	13469	14244	12468	89125	76946
$M_a = 10$ GeV	15476	12157	13054	11418	81639	70531
$M_a = 100$ GeV	7199	4582	6011	4569	35675	26497

TABLE V. Exploring ALP-$\gamma\gamma$ vertex: Total signal and BG event count before and after $PT_{\gamma\gamma} > 50$ GeV with $g_{a\gamma\gamma} = 4.88 \times 10^{-3}$.

	$e^+e^- \to e^+e^-\gamma\gamma$		$e^+e^- \to \mu^+\mu^-\gamma\gamma$	
	Before cut	After cut	Before cut	After cut
BG	101540	26225	27200	12269
$M_a = 0.1$ GeV	390458	306706	13441	11747
$M_a = 1$ GeV	387248	305312	13247	11595
$M_a = 10$ GeV	352115	276587	12148	10625
$M_a = 100$ GeV	203630	129625	6869	5221

TABLE VI. Exploring ALP-WW vertex: Total signal and BG event count before and after $PT_{\gamma\gamma} > 50$ GeV with $g_{aWW} = 8 \times 10^{-3}$.

	$e^+e^- \to \nu\bar{\nu}\gamma\gamma$	
	Before cut	After cut
BG	107200	49727
$M_a = 0.1$ GeV	31333	27081
$M_a = 1$ GeV	30981	26747
$M_a = 10$ GeV	28168	24336
$M_a = 100$ GeV	8718	6475

$$Z = \sqrt{2.\left[(s+b)\ln\left(\frac{(s+b)(b+\sigma_b^2)}{b^2+(s+b)\sigma_b^2}\right) - \frac{b^2}{\sigma_b^2}\ln\left(1+\frac{\sigma_b^2 s}{b(b+\sigma_b^2)}\right)\right]}, \tag{10}$$

where the numbers of signal and background events are represented by s and b, respectively. The systematic uncertainty associated with the SM background b is denoted by σ_b. A significance value of $Z = 2$ is considered, which corresponds to 95% confidence level (C.L.). In the following subsections, we discuss the sensitivity of the ALP couplings from ALP production with three different leptonic final states at the Higgs factory.

A. $e^+e^- \to e^+e^-a, a \to \gamma\gamma$

The process of ALP production, in conjunction with a pair of electrons mediated by γ and Z bosons, is illustrated in Fig. 1. In this process, the effective couplings of the ALP to ZZ, $\gamma\gamma$, and γZ are associated with the dimensional couplings g_{aZZ}, $g_{a\gamma\gamma}$, and $g_{aZ\gamma}$, respectively. The numbers of signal and background events are estimated using Eqs. (8) and (9), and are shown in the left panel of Fig. 4.

The combination of production via photon fusion followed by the ALP decay into diphoton yields the highest number of signal events for the specified value of $g_{a\gamma\gamma}$ coupling listed in Table II. The number of ALP events from the ALP-ZZ vertex is intermediate, while the ALP-$Z\gamma$ vertex gives the least number of events, even the SM event rate is higher than the latter one. The kinks in the number of signal event curves arise from the branching ratio of the ALP into diphoton $a \to \gamma\gamma$.

We then estimate the sensitivity in the ALP couplings versus the ALP mass, especially $g_{a\gamma\gamma}$ and g_{aZZ} using Eq. (10). We account for the systematic uncertainty associated with the background estimation by including assuming an uncertainty of $\sigma_b = 10\%$. The bounds on the ALP couplings $g_{a\gamma\gamma}$ (blue) and g_{aZZ} (orange) as a function of the ALP mass M_a are shown in the right panel of Fig. 4. It is easy to see that the sensitivity of the $g_{a\gamma\gamma}$ coupling is a few times better than the g_{aZZ} coupling. At lighter ALP mass of $M_a = 0.1$ GeV, the sensitivity of $g_{a\gamma\gamma}$ can

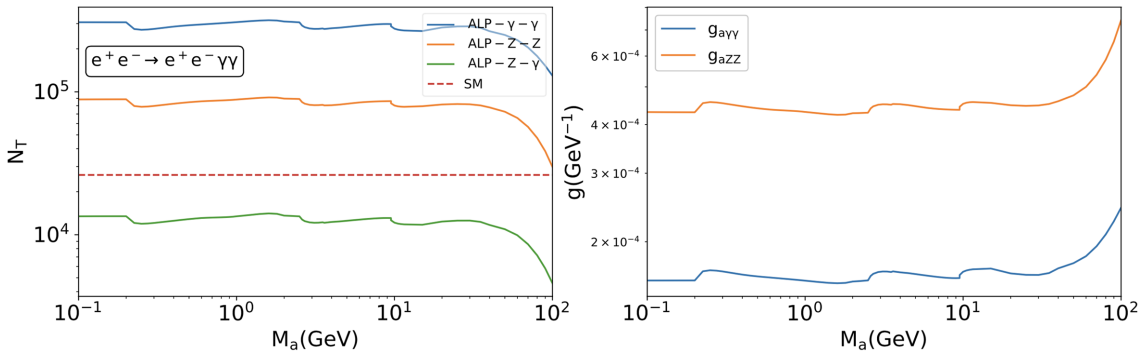

FIG. 4. Left panel: the number of ALP events from the channel $e^+e^- \to e^+e^-a$ followed by $a \to \gamma\gamma$ (event rates are estimated with the coupling strengths listed in Table II: $g_{a\gamma\gamma} = 4.88 \times 10^{-3}$ GeV^{-1}, $g_{aZ\gamma} = 1.38 \times 10^{-3}$ GeV^{-1}, and $g_{aZZ} = 7.11 \times 10^{-3}$ GeV^{-1}). Right panel: the 95% C.L. sensitivity curves on $g_{a\gamma\gamma}$ (solid blue) and g_{aZZ} (solid orange) for $e^+e^- \to e^+e^-a, a \to \gamma\gamma$.

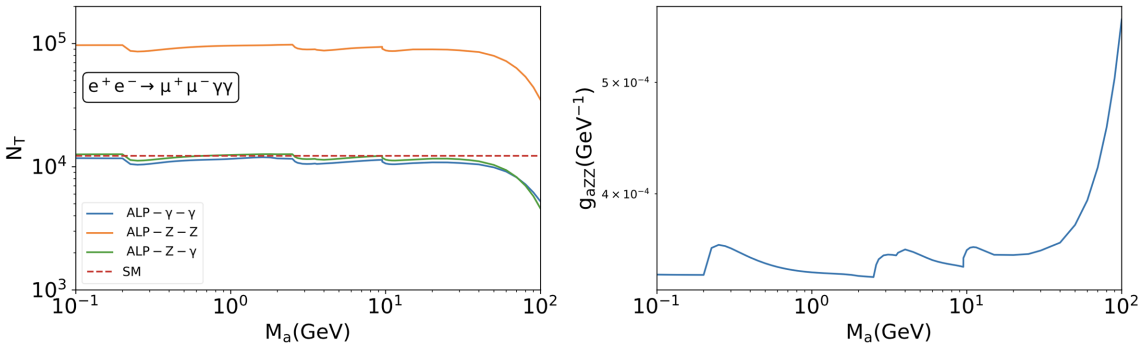

FIG. 5. Left panel: the number of ALP events from the channel $e^+e^- \to \mu^+\mu^- a$ followed by $a \to \gamma\gamma$ (event rates are estimated with the coupling strengths listed in Table II: $g_{a\gamma\gamma} = 4.88 \times 10^{-3}$ GeV^{-1}, $g_{aZ\gamma} = 1.38 \times 10^{-3}$ GeV^{-1}, and $g_{aZZ} = 7.11 \times 10^{-3}$ GeV^{-1}). Right panel: the 95% C.L. sensitivity curve of g_{aZZ} (solid blue) for $e^+e^- \to \mu^+\mu^- a, a \to \gamma\gamma$.

reach down to $\sim 1.5 \times 10^{-4}$ GeV^{-1}, while g_{aZZ} reaches down to $\sim 4.3 \times 110^{-4}$ GeV^{-1}. The sensitivity curves stay more or less flat until $M_a = 30$ GeV with some irregularities due to the branching ratio into diphoton. As M_a increases beyond 30 GeV, the sensitivity is largely worsened due to smaller phase space for the production of heavier ALPs. At $M_a = 100$ GeV, the bounds on $g_{a\gamma\gamma}$ and g_{aZZ} are reduced to approximately 2.5×10^{-4} GeV^{-1} and 7.5×10^{-4} GeV^{-1}, respectively.

B. $e^+e^- \to \mu^+\mu^- a, a \to \gamma\gamma$

Here we consider the associated production of the ALP with a $\mu^+\mu^-$ pair. This process only arises from s-channel diagrams listed in Fig. 1. The left panel of Fig. 5 shows the number of ALP events arising from various ALP vertices. The highest number of ALP events comes from ALP production associated with the ALP-ZZ vertex. The numbers of ALP events produced via the ALP-$Z\gamma$ and ALP-$\gamma\gamma$ vertices are lower than that of the SM. The right panel of Fig. 5 shows the sensitivity reach of the g_{aZZ} coupling as a function of ALP mass M_a. The effect of the diphoton branching ratio also reflects in the sensitivity curves. At $M_a = 0.1$ GeV, g_{aZZ} can be probed down to $\sim 3.4 \times 10^{-4}$ GeV^{-1}. The sensitivity of g_{aZZ} weakens with the increment of the ALP mass, especially for M_a above 30 GeV.

Comparing the bounds of g_{aZZ} obtained in the channels $e^+e^- \to \mu^+\mu^- a$ (Fig. 5) and $e^+e^- \to e^+e^- a$ (Fig. 4), we can see that g_{aZZ} from the muon channel performs better than the electron channel over the entire ALP mass range. This is simply because the background in the muon channel is only a fraction of the electron channel.

C. $e^+e^- \to \nu\bar{\nu} a, a \to \gamma\gamma$

As already shown in Fig. 2, the channel $e^+e^- \to \nu\bar{\nu} a$ with $a \to \gamma\gamma$ has the largest cross sections compared to the other two processes. This process also presents an opportunity to investigate the ALP-WW vertex. In addition to the ALP-WW vertex, the ALP-ZZ and ALP-$Z\gamma$ vertices also make contributions, which are depicted in Fig. 1.

The number of ALP events from the ALP-ZZ vertex is higher than that from the other two vertices. The ALP production rate from the ALP-WW vertex is the lowest and is even lower than that of the SM.

The bounds on g_{aZZ} and $g_{aZ\gamma}$ couplings are shown in the right panel of Fig. 6. In this case, the $g_{aZ\gamma}$ coupling

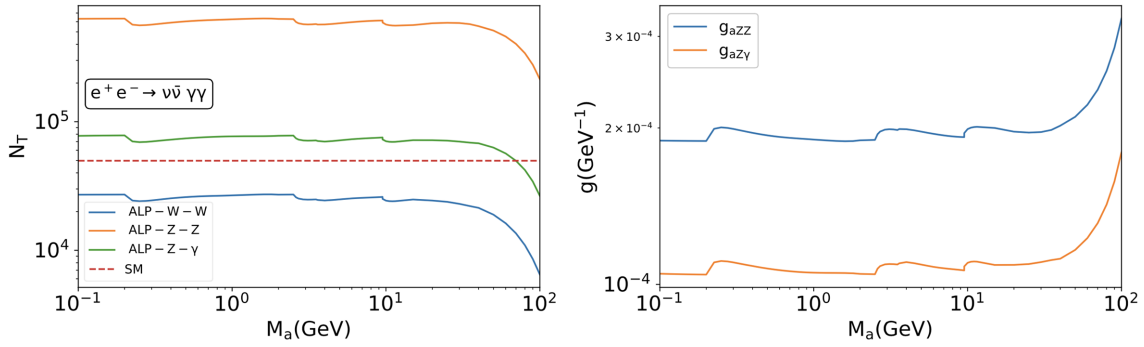

FIG. 6. Left panel: the number of ALP events from $e^+e^- \to \nu\bar{\nu} a$, followed by $a \to \gamma\gamma$ (event rates are estimated with the coupling strengths listed in Table II: $g_{aZ\gamma} = 1.38 \times 10^{-3}$ GeV^{-1}, $g_{aZZ} = 7.11 \times 10^{-3}$ GeV^{-1}, and $g_{aWW} = 8 \times 10^{-3}$ GeV^{-1}). Right panel: the 95% C.L. sensitivity curves on g_{aZZ} (solid blue) and $g_{aZ\gamma}$ (solid orange) for $e^+e^- \to \nu\bar{\nu} a, a \to \gamma\gamma$.

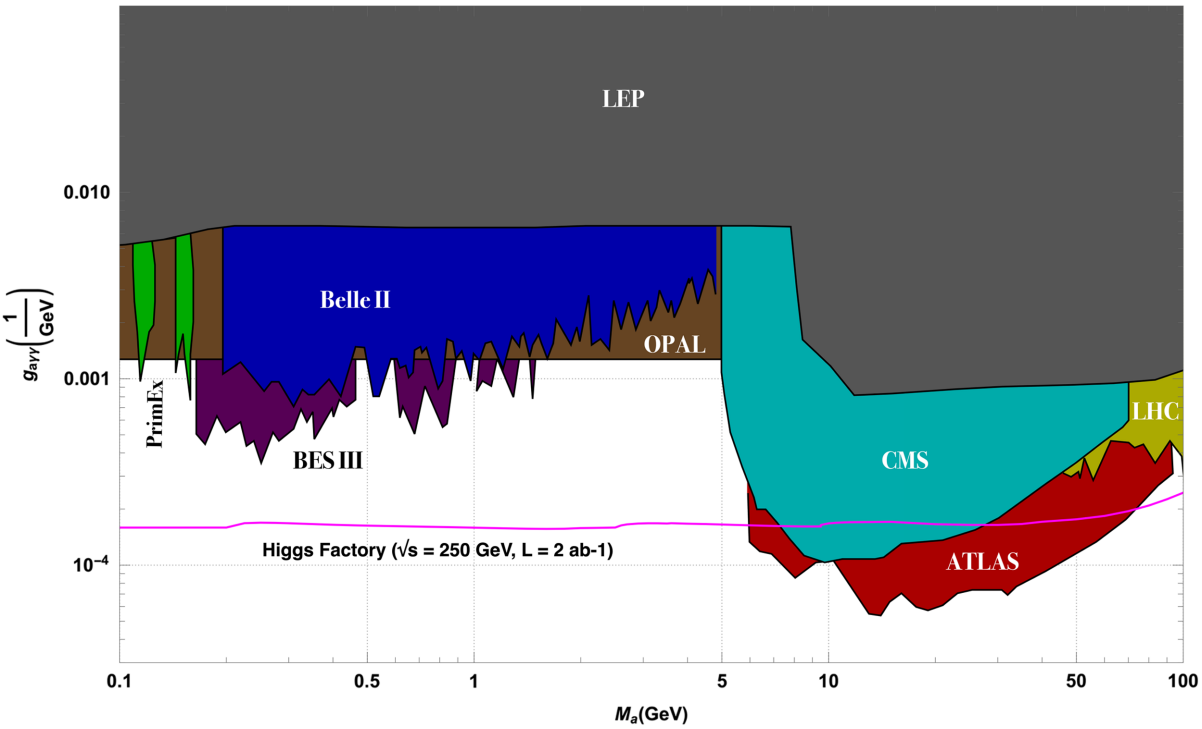

FIG. 7. Summary plot of the sensitivity of $g_{a\gamma\gamma}$ that we can achieve at the Higgs factory $\sqrt{s} = 250$ GeV with an integrated luminosity 2 ab^{-1}, and compared with other existing constraints. Existing constraints in the figure include PrimEx [56], BES III [57], Belle II [49], LEP [29], OPAL [58], CMS [59], ATLAS [60], and LHC [58] (extracted from the GitHub page [61]).

has a better bound compared to the g_{aZZ} coupling. At $M_a = 0.1$ GeV, the $g_{aZ\gamma}$ coupling can reach down to $\sim 10^{-4}$ GeV^{-1}, while the g_{aZZ} coupling reaches down to 1.8×10^{-4} GeV^{-1}. Similar to previous cases, the sensitivity of the couplings weakens as the ALP mass M_a increases.

When comparing the bounds of g_{aZZ} coupling obtained from all different channels the best sensitivity comes from $e^+e^- \to \nu\bar{\nu}a, a \to \gamma\gamma$. At $M_a = 0.1$ GeV, the g_{aZZ} coupling reaches down to 1.8×110^{-4} GeV^{-1}. The $e^+e^- \to e^+e^-a, a \to \gamma\gamma$ channel offers the least sensitivity (for $M_a = 0.1$ GeV g_{aZZ} coupling only reaches down to 4.3×110^{-4} GeV^{-1}). The limit from the $e^+e^- \to \mu^+\mu^-a, a \to \gamma\gamma$ channel is intermediate (for $M_a = 0.1$ GeV the g_{aZZ} coupling reaches down to 3.4×110^{-4} GeV^{-1}). This trend is visible across the entire ALP mass range from $M_a = 0.1$ to 100 GeV.

V. CONCLUSIONS

In this study, we have explored the sensitivity potential of the future Higgs factories, including ILC, CEPC, and FCC-ee, on probing dimensionful coupling constants $g_{a\gamma\gamma}$, $g_{aZ\gamma}$, g_{aWW}, and g_{aZZ} of the axionlike particle, via the processes $e^+e^- \to f\bar{f}a(f = e, \mu, \nu)$ followed by $a \to \gamma\gamma$. We used a center-of-mass energy $\sqrt{s} = 250$ GeV with an integrated luminosity 2 ab^{-1}.

Our results have shown that the channel $e^+e^- \to e^+e^-a$, $a \to \gamma\gamma$ provides the best bound for the $g_{a\gamma\gamma}$ coupling, while the process $e^+e^- \to \nu\bar{\nu}a$, $a \to \gamma\gamma$ offers the best bound for the g_{aZZ} and $g_{aZ\gamma}$ couplings.

Without loss of generality, we have used $C_{WW} = 2$ and $C_{BB} = 1$ such that $g_{a\gamma\gamma}$, $g_{aZ\gamma}$, g_{aWW}, and g_{aZZ} are related to one another shown in Eqs. (4)–(7), and they are all nonzero. We can easily extend the analysis to independent coupling strengths.

Finally, we show in Fig. 7 the summary plot of the sensitivity of $g_{a\gamma\gamma}$ that we can achieve at the Higgs factories, and compared with other existing constraints. The sensitivity can improve down to about 1.5×10^{-4} GeV^{-1} over the mass range of $M_a = 0.1$–6 GeV, as well as a small corner at $M_a \simeq 70$–100 GeV.

Our estimates of the bounds for the $g_{a\gamma\gamma}$, $g_{aZ\gamma}$, and g_{aZZ} couplings as a function of ALP mass (M_a) ranging from 0.1 to 100 GeV provide valuable insights for future experiments aiming to detect ALPs.

Note that the decay of the ALP in this work is prompt or mostly prompt. The decay length of the ALP is calculated in Appendix A and shown in Fig. 8 with the value of $g_{a\gamma\gamma} = 4.88 \times 10^3$ GeV^{-1}. Even the limits of $g_{a\gamma\gamma}$ that we obtain in Fig. 7 the longest decay length of the ALP with a mass of 0.1 GeV is of order 10^{-2} cm, which is mostly prompt. Therefore, we only consider prompt decay in this work.

ACKNOWLEDGMENTS

Special thanks to Zeren Simon Wang, Nguyen Tran Quang Thong, and Chih-Ting Lu for enlightening discussion. The work was supported in part by NSTC under Grant No. MOST-110-2112-M-007-017-MY3.

APPENDIX A: PARTIAL DECAY WIDTHS AND BRANCHING RATIOS OF THE ALP

The two-body partial decay widths of the ALP to photons and fermions are given below. The branching ratios are evaluated with $C_{BB} = 1$, $C_{WW} = 2$, $C_{a\phi} = 1$, and $f_a = 1000$ GeV. Here M_l and M_q are the masses of charged leptons and quarks.

$$\Gamma(a \to \gamma\gamma) = \frac{M_a^6 (C_{BB} c_w^2 + C_{WW} s_w^2)^2}{4 f_a^2 \pi |M_a^3|}, \tag{A1}$$

$$\Gamma(a \to l\bar{l}) = \frac{c_{a\phi}^2 M_a^2 \sqrt{M_a^2 - 4M_a^2 M_l^2}\, v e v^2 y_l^2}{16\pi f_a^2 |M_a^3|}, \tag{A2}$$

$$\Gamma(a \to q\bar{q}) = \frac{3 c_{a\phi}^2 M_a^2 \sqrt{M_a^2 - 4M_a^2 M_q^2}\, v e v^2 y_q^2}{16\pi f_a^2 |M_a^3|}, \tag{A3}$$

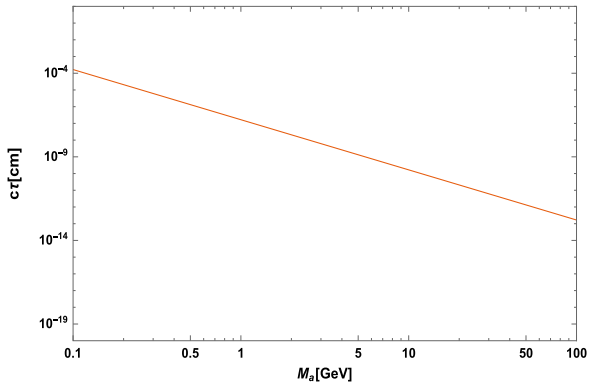

FIG. 8. Decay length of ALP with $g_{a\gamma\gamma} = 4.88 \times 10^{-3}$ GeV^{-1} ($C_{WW} = 2$, $C_{BB} = 1$, and $f_a = 1$ TeV).

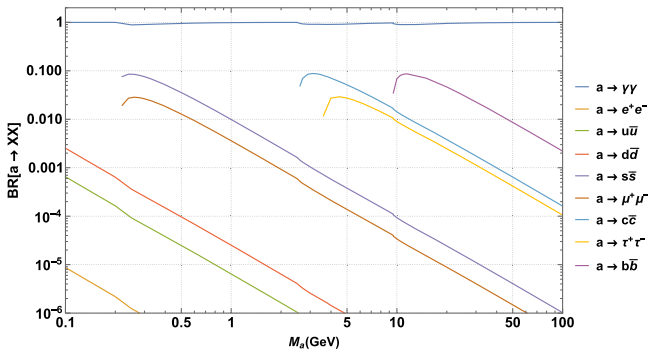

FIG. 9. Branching ratios of the ALP with $C_{WW} = 2$, $C_{BB} = 1$, and $f_a = 1$ TeV.

$$\Gamma^{\mathrm{Tot}}(a) \sim \Gamma(a \to \gamma\gamma). \tag{A4}$$

The total decay width Γ^{Tot} of the ALP is approximately equal to the partial decay width of the ALP into a pair of photons $\Gamma(a \to \gamma\gamma)$. The decay length of the ALP is shown in Fig. 9.

APPENDIX B: DERIVATION OF THE FORMULAS FOR THE SIGNIFICANCE

Poisson likelihood function for the parameter s (where s is the number of signal events and b stands for the number of background events) is given by

$$L(s) = \frac{(s+b)^n}{n!} e^{-(s+b)}. \tag{B1}$$

Using the method of maximum likelihood, $L(s)$ attains the maximum at $s = \hat{s}$ such that

$$\left.\frac{\partial \ln L(s)}{\partial s}\right|_{s=\hat{s}} = \frac{n}{\hat{s}+b} = 0, \quad \Rightarrow \hat{s} = n - b. \tag{B2}$$

The likelihood-ratio statistics for testing the hypothesis $s = 0$ is

$$q_0 = -2 \ln\left(\frac{L(s=0)}{L(\hat{s})}\right). \tag{B3}$$

Substituting $\hat{s} = n - b$ we obtain

$$q_0 = -2\left[n \ln\left(\frac{b}{n}\right) - (b-n)\right].$$

To find the median significance $Z = \sqrt{q_0}$ we set $n \to s + b$ (i.e., the Asimov dataset):

$$Z = \sqrt{2\left[(s+b)\ln\left(1 + \frac{s}{b}\right) - s\right]}. \tag{B4}$$

In the case that the number of background events is uncertain, which is accounted for by the systematic uncertainty. We can treat the number of background events b as a nuisance parameter. The likelihood-ratio statistics q_0 is then given by

$$q_0 = \begin{cases} -2 \ln \lambda(0), & \text{for } \hat{s} \geq 0 \\ 0, & \text{for } \hat{s} < 0 \end{cases}, \tag{B5}$$

where

$$\lambda(s) = \frac{L(s, \hat{\hat{b}}(s))}{L(\hat{s}, \hat{b})}, \tag{B6}$$

where $L(s,b)$ attains the maximum at $s=\hat{s}$ and $b=\hat{b}$, and $L(s,\hat{\hat{b}}(s))$ is where L attains a maximum for $s\neq\hat{s}$ at $b=\hat{\hat{b}}(s)$.

For two Poisson-distributed values: $n\sim$ Poisson $(s+b)$ and $m\sim$ Poisson (τb), the likelihood function is

$$L(s,b)=\frac{(s+b)^n}{n!}e^{-(s+b)}\frac{(\tau b)^m}{m!}e^{-(\tau b)}. \tag{B7}$$

Setting $\partial L(s,b)/\partial s=\partial L(s,b)/\partial b=0$ simultaneously, we obtain

$$\hat{s}=n-b,\qquad \hat{b}=\frac{m}{\tau}. \tag{B8}$$

On the other hand, for $s\neq\hat{s}$, $L(s,b)$ attains a maximum at $b=\hat{\hat{b}}(s)$, which is given by

$$\hat{\hat{b}}(s)=\frac{1}{2(1+\tau)}\left[n+m-(1+\tau)s+\sqrt{(n+m-(1+\tau)s)^2+4(1+\tau)ms}\right], \tag{B9}$$

where we have taken the positive square root to account for a positive b.

The likelihood-ratio statistics for testing the hypothesis $s=0$ is given by

$$q_0=-2\ln\lambda(s=0)=-2\ln\frac{L(0,\hat{\hat{b}}(0))}{L(\hat{s},\hat{b})}. \tag{B10}$$

Using this likelihood-ratio statistics we obtain the significance

$$Z=\sqrt{q_0}=\left\{-2\left[n\ln\left(\frac{(n+m)}{(1+\tau)n}\right)+m\ln\left(\frac{\tau(n+m)}{(1+\tau)m}\right)\right]\right\}^{1/2}. \tag{B11}$$

To obtain the median significance we replace $n\to s+b$ and $m\to\tau b$. We also eliminate τ by setting the variance of $\hat{b}$ given by $V(\hat{b})\equiv\sigma_b^2=b/\tau$, we arrive in the following formula

$$Z=\left\{2\left[(s+b)\ln\left(\frac{(s+b)(b+\sigma_b^2)}{b^2+(s+b)\sigma_b^2}\right)-\frac{b^2}{\sigma_b^2}\ln\left(1+\frac{\sigma_b^2 s}{b(b+\sigma_b^2)}\right)\right]\right\}^{1/2}. \tag{B12}$$

[1] R. D. Peccei and H. R. Quinn, *CP* Conservation in the Presence of Instantons, Phys. Rev. Lett. **38**, 1440 (1977).

[2] S. Weinberg, A New Light Boson?, Phys. Rev. Lett. **40**, 223 (1978).

[3] F. Wilczek, Problem of Strong P and T Invariance in the Presence of Instantons, Phys. Rev. Lett. **40**, 279 (1978).

[4] J. Preskill, M. B. Wise, and F. Wilczek, Cosmology of the invisible axion, Phys. Lett. B **120**, 127 (1983).

[5] L. F. Abbott and P. Sikivie, A cosmological bound on the invisible axion, Phys. Lett. B **120**, 133 (1983).

[6] M. Dine and W. Fischler, The not so harmless axion, Phys. Lett. B **120**, 137 (1983).

[7] F. Takahashi, W. Yin, and A. H. Guth, QCD axion window and low-scale inflation, Phys. Rev. D **98**, 015042 (2018).

[8] G. Aarons *et al.* (ILC Collaboration), International linear collider reference design report volume 2: Physics at the ILC, arXiv:0709.1893.

[9] M. Ahmad *et al.*, CEPC-SPPC preliminary conceptual design report. 1. Physics and detector, Report No. IHEP-CEPC-DR-2015-01, IHEP-TH-2015-01, IHEP-EP-2015-01, 2015.

[10] A. Abada *et al.* (FCC Collaboration), FCC-ee: The Lepton Collider: Future circular collider conceptual design report volume 2, Eur. Phys. J. Special Topics **228**, 261 (2019).

[11] M. Bauer, M. Heiles, M. Neubert, and A. Thamm, Axion-like particles at future colliders, Eur. Phys. J. C **79**, 74 (2019).

[12] I. Brivio, M. B. Gavela, L. Merlo, K. Mimasu, J. M. No, R. del Rey, and V. Sanz, ALPs effective field theory and collider signatures, Eur. Phys. J. C **77**, 572 (2017).

[13] H. Georgi, D. B. Kaplan, and L. Randall, Manifesting the invisible axion at low-energies, Phys. Lett. B **169**, 73 (1986).

[14] J. Ren, D. Wang, L. Wu, J. M. Yang, and M. Zhang, Detecting an axion-like particle with machine learning at the LHC, J. High Energy Phys. 11 (2021) 138.
[15] K. A. Olive *et al.* (Particle Data Group Collaboration), Review of particle physics, Chin. Phys. C **38**, 090001 (2014).
[16] N. Vinyoles, A. Serenelli, F. L. Villante, S. Basu, J. Redondo, and J. Isern, New axion and hidden photon constraints from a solar data global fit, J. Cosmol. Astropart. Phys. 10 (2015) 015.
[17] G. G. Raffelt, Astrophysical axion bounds, Lect. Notes Phys. **741**, 51 (2008).
[18] A. Friedland, M. Giannotti, and M. Wise, Constraining the Axion-Photon Coupling with Massive Stars, Phys. Rev. Lett. **110**, 061101 (2013).
[19] A. Ayala, I. Domínguez, M. Giannotti, A. Mirizzi, and O. Straniero, Revisiting the Bound on Axion-Photon Coupling from Globular Clusters, Phys. Rev. Lett. **113**, 191302 (2014).
[20] V. Khachatryan *et al.* (CMS Collaboration), Search for dark matter, extra dimensions, and unparticles in monojet events in proton–proton collisions at $\sqrt{s} = 8$ TeV, Eur. Phys. J. C **75**, 235 (2015).
[21] G. Aad *et al.* (ATLAS Collaboration), Search for new phenomena in final states with an energetic jet and large missing transverse momentum in pp collisions at $\sqrt{s} =$ 8 TeV with the ATLAS detector, Eur. Phys. J. C **75**, 299 (2015); **75**, 408(E) (2015).
[22] E. Aprile *et al.* (XENON100 Collaboration), First axion results from the XENON100 experiment, Phys. Rev. D **90**, 062009 (2014); **95**, 029904(E) (2017).
[23] N. Viaux, M. Catelan, P. B. Stetson, G. Raffelt, J. Redondo, A. A. R. Valcarce, and A. Weiss, Neutrino and Axion Bounds from the Globular Cluster M5 (NGC 5904), Phys. Rev. Lett. **111**, 231301 (2013).
[24] M. Tian, Z. S. Wang, and K. Wang, Search for long-lived axions with far detectors at future lepton colliders, arXiv: 2201.08960.
[25] L. Calibbi, Z. Huang, S. Qin, Y. Yang, and X. Yin, Testing axion couplings to leptons in Z decays at future e^+e^- colliders, Phys. Rev. D **108**, 015002 (2023).
[26] K. Sakurai and W. Yin, Phenomenology of *CP*-even ALP, J. High Energy Phys. 04 (2022) 113.
[27] G. Haghighat, M. Mohammadi Najafabadi, K. Sakurai, and W. Yin, Probing a light dark sector at future lepton colliders via invisible decays of the SM-like and dark Higgs bosons, Phys. Rev. D **107**, 035033 (2023).
[28] C.-T. Lu, Lighting electroweak-violating ALP-lepton interactions at e^+e^- and ep colliders, arXiv:2210.15648.
[29] J. Jaeckel and M. Spannowsky, Probing MeV to 90 GeV axion-like particles with LEP and LHC, Phys. Lett. B **753**, 482 (2016).
[30] M. J. Dolan, F. Kahlhoefer, C. McCabe, and K. Schmidt-Hoberg, A taste of dark matter: Flavour constraints on pseudoscalar mediators, J. High Energy Phys. 03 (2015) 171; 07 (2015) 103(E).
[31] E. Izaguirre, T. Lin, and B. Shuve, Searching for Axionlike Particles in Flavor-Changing Neutral Current Processes, Phys. Rev. Lett. **118**, 111802 (2017).
[32] D. d'Enterria, Collider constraints on axion-like particles, in Workshop on Feebly Interacting Particles (2021), 2, arXiv: 2102.08971.
[33] M. Bauer, M. Neubert, and A. Thamm, LHC as an Axion Factory: Probing an Axion Explanation for $(g-2)_\mu$ with Exotic Higgs Decays, Phys. Rev. Lett. **119**, 031802 (2017).
[34] D. J. E. Marsh, Axion cosmology, Phys. Rep. **643**, 1 (2016).
[35] P. Arias, D. Cadamuro, M. Goodsell, J. Jaeckel, J. Redondo, and A. Ringwald, WISPy cold dark matter, J. Cosmol. Astropart. Phys. 06 (2012) 013.
[36] J. Jaeckel, J. Redondo, and A. Ringwald, 3.55 keV hint for decaying axionlike particle dark matter, Phys. Rev. D **89**, 103511 (2014).
[37] E. Aprile *et al.* (XENON Collaboration), Excess electronic recoil events in XENON1T, Phys. Rev. D **102**, 072004 (2020).
[38] C. Gao, J. Liu, L.-T. Wang, X.-P. Wang, W. Xue, and Y.-M. Zhong, Reexamining the Solar Axion Explanation for the XENON1T Excess, Phys. Rev. Lett. **125**, 131806 (2020).
[39] E. Aprile *et al.* (XENON Collaboration), Search for New Physics in Electronic Recoil Data from XENONnT, Phys. Rev. Lett. **129**, 161805 (2022).
[40] M. J. Dolan, T. Ferber, C. Hearty, F. Kahlhoefer, and K. Schmidt-Hoberg, Revised constraints and Belle II sensitivity for visible and invisible axion-like particles, J. High Energy Phys. 12 (2017) 094; 03 (2021) 190(E).
[41] M. Bauer, M. Neubert, S. Renner, M. Schnubel, and A. Thamm, Axionlike Particles, Lepton-Flavor Violation, and a New Explanation of a_μ and a_e, Phys. Rev. Lett. **124**, 211803 (2020).
[42] D. Banerjee *et al.* (NA64 Collaboration), Search for Axion-like and Scalar Particles with the NA64 Experiment, Phys. Rev. Lett. **125**, 081801 (2020).
[43] L. Calibbi, D. Redigolo, R. Ziegler, and J. Zupan, Looking forward to lepton-flavor-violating ALPs, J. High Energy Phys. 09 (2021) 173.
[44] F. Björkeroth, E. J. Chun, and S. F. King, Flavourful axion phenomenology, J. High Energy Phys. 08 (2018) 117.
[45] S. Chakraborty, M. Kraus, V. Loladze, T. Okui, and K. Tobioka, Heavy QCD axion in b → s transition: Enhanced limits and projections, Phys. Rev. D **104**, 055036 (2021).
[46] B. Döbrich, J. Jaeckel, F. Kahlhoefer, A. Ringwald, and K. Schmidt-Hoberg, ALPtraum: ALP production in proton beam dump experiments, J. High Energy Phys. 02 (2016) 018.
[47] W. J. Marciano, A. Masiero, P. Paradisi, and M. Passera, Contributions of axionlike particles to lepton dipole moments, Phys. Rev. D **94**, 115033 (2016).
[48] S. Gori, G. Perez, and K. Tobioka, KOTO vs. NA62 dark scalar searches, J. High Energy Phys. 08 (2020) 110.
[49] F. Abudinén *et al.* (Belle-II Collaboration), Search for Axion-Like Particles Produced in e^+e^- Collisions at Belle II, Phys. Rev. Lett. **125**, 161806 (2020).
[50] N. Steinberg and J. D. Wells, Axion-like particles at the ILC Giga-Z, J. High Energy Phys. 08 (2021) 120.
[51] N. Steinberg, Discovering axion-like particles with photon fusion at the ILC, arXiv:2108.11927.

[52] C.-X. Yue, H.-Y. Zhang, and H. Wang, Production of axion-like particles via vector boson fusion at future electron-positron colliders, Eur. Phys. J. C **82**, 88 (2022).
[53] J. Alwall, M. Herquet, F. Maltoni, O. Mattelaer, and T. Stelzer, MadGraph 5: Going beyond, J. High Energy Phys. 06 (2011) 128.
[54] J. Alwall, R. Frederix, S. Frixione, V. Hirschi, F. Maltoni, O. Mattelaer, H. S. Shao, T. Stelzer, P. Torrielli, and M. Zaro, The automated computation of tree-level and next-to-leading order differential cross sections, and their matching to parton shower simulations, J. High Energy Phys. 07 (2014) 079.
[55] A. Arhrib, K. Cheung, and C.-T. Lu, Same-sign charged Higgs boson pair production in bosonic decay channels at the HL-LHC and HE-LHC, Phys. Rev. D **102**, 095026 (2020).
[56] D. Aloni, C. Fanelli, Y. Soreq, and M. Williams, Photoproduction of Axionlike Particles, Phys. Rev. Lett. **123**, 071801 (2019).
[57] M. Ablikim *et al.* (BESIII Collaboration), Search for an axion-like particle in radiative J/ψ decays, Phys. Lett. B **838**, 137698 (2023).
[58] S. Knapen, T. Lin, H. K. Lou, and T. Melia, Searching for Axionlike Particles with Ultraperipheral Heavy-Ion Collisions, Phys. Rev. Lett. **118**, 171801 (2017).
[59] A. M. Sirunyan *et al.* (CMS Collaboration), Evidence for light-by-light scattering and searches for axion-like particles in ultraperipheral PbPb collisions at $\sqrt{s_{\mathrm{NN}}} = 5.02$ TeV, Phys. Lett. B **797**, 134826 (2019).
[60] G. Aad *et al.* (ATLAS Collaboration), Measurement of light-by-light scattering and search for axion-like particles with 2.2 nb^{-1} of $\mathrm{Pb}+\mathrm{Pb}$ data with the ATLAS detector, J. High Energy Phys. 03 (2021) 243; 11 (2021) 50.
[61] C. O'Hare, cajohare/axionlimits: Axionlimits, https://cajohare.github.io/AxionLimits/, July, 2020.